Article

Journal of the Brazilian Chemical Society

https://dx.doi.org/10.21577/0103-5053.20240201

J. Braz. Chem. Soc. **2025**, *36*, 5, e-20240201, 1-10

Novel Terpene-Reinforced Photopolymerizable Resins Derived from Methacrylate Salts of Imidazole

Ilária M. S. Lins,[a] Anderson G. Vieira,[a] Rubson P. S. Ribeiro,[a] Dayane K. D. N. Santos,[a] Larissa G. Maciel,[a] Petrus A. Santa-Cruz,[a] Severino Alves Júnior[a] and Janaína V. dos Anjos[*,a]

[a]Departamento de Química Fundamental, Universidade Federal de Pernambuco, 50740-560 Recife-PE, Brazil

This research aims to develop new 3D (three-dimensional) printable resins made from methacrylate salts of imidazole, 2-methyl-imidazole, and 1-methyl-imidazole, with glycerol trimethacrylate serving as a crosslinking agent. With their backbone structure, these resins are easy and rapid to prepare, offering an alternative to conventional ones. Reinforced with terpene-based additives such as α-pinene, (*R*)-limonene, *trans*-ethyl cinnamate, and safrole, they present a diverse range of fifteen resin formulations. Each resin underwent printability tests, including printing tests, which revealed accuracy, precision, and dimensional stability compared to a commercial resin and its respective digital 3D models. Mechanical tests further demonstrated that adding alpha-pinene and (*R*)-limonene enhanced hardness, while safrole had the opposite effect. Resins containing α-pinene and (*R*)-limonene as additives showcased an elasticity modulus comparable to the commercial resin. According to mechanical tests, a cytocompatibility assay was conducted for the best resin, showing that this resin holds potential for developing drug delivery systems and other biomedical devices.

Keywords: additive manufacturing, imidazole salts, glycerol methacrylate, terpenes, drug delivery systems

Introduction

Additive manufacturing (AM), ordinarily known as 3D (three-dimensional) printing, covers a range of processes enabling the (3D) fabrication of objects by adding material layer by layer directly from computer-generated model data.[1,2] AM eliminates typical steps in traditional manufacturing methods, such as cutting, casting, forging, and mold-making.[3] This technology opens new possibilities for complex geometries and mass customization of parts at commercially viable costs. Additionally, it allows for incorporating new features into medical devices,[4] which can benefit patient care across various therapeutic areas.[5]

Stereolithography (SLA) enables the production of objects from a photosensitive resin using an LED (light emitting diode) source. The localized photopolymerization process is triggered by digitally projecting light patterns onto the liquid surface.[6] Among the available 3D printing technologies, those based on liquid resins, such as stereolithography, offer higher resolution and precision than others. The selective and rapid conversion of liquid monomers or oligomers into solid polymers after light curing forms the basis of these techniques.[7]

The MSLA, or masked stereolithography apparatus, is a modified version of SLA 3D printing that operates on a similar principle of curing liquid resin with light. However, the MSLA method differs slightly in using a more prominent light source selectively masked with an LCD (liquid crystal display) screen to create the desired object. Unlike traditional SLA 3D printers that rely on the number of layers and material in each layer to be cured with a laser, MSLA technology depends solely on the number of printed layers. This gives MSLA printers an advantage in curing speed, particularly when printing multiple objects simultaneously. In SLA machines, the laser beam diameter determines the resolution, while MSLA resolution depends on the resolution of the LCD screen.[8] The liquid containing the polymerizable material is commonly referred to as resin. An SLA resin must contain two essential components: monomers or oligomers and a photoinitiator, which can be either cationic or free radical. Some resins may contain additives such as plasticizers, dyes, flavorings, or substances to confer additional functionalities like drugs or natural products.[9]

*e-mail: janaina.anjos@ufpe.br
Editor handled this article: Célia M. Ronconi (Associate)

Monomers and oligomers are compounds with molecules containing groups that polymerize upon light exposure and radical formation to form the desired object.[10]

Methacrylates are α, β-unsaturated derivatives of methacrylic and are widely employed in the industry. The unsaturation is highly polarized, and the electron density of the double bond is reduced by proximity to the carbonyl, which exerts electron withdrawing and mesomeric effects. This renders methacrylates susceptible to electrophilic, nucleophilic, and free radical attacks. Radicals formed in methacrylates are resonance-stabilized, making this type of radical-mediated reaction a preferred route for forming polymers of this nature.[11]

Acrylic resins are typically associated with toxicity or unpleasant odors, leading to modifications to make them less toxic, more environmentally friendly, and more pleasant to work with in enclosed spaces due to their pungent smell.[12] One of the simplest ways to modify methacrylic acids is to transform them into salts. These salts tend to be odorless and more soluble in water and other solvents while maintaining the usual polymerization capacity of methacrylates.[13] However, most methacrylate salts are solids at room temperature. This hinders the vat polymerization process, as the resins should be liquid, and solid salts would have to be dissolved in some solvent. Nevertheless, imidazole salts of methacrylates have been reported in recent literature[14] as the main component of resins for SLA/MSLA, with the advantage of being liquid salts at room temperature. Additionally, imidazole salts are typically non-toxic and associated with antimicrobial activity, potentially leading to self-decontaminating materials.[15]

Terpenes are essential compounds due to their diverse structural features and chemical and physical properties. They are of significant interest for applications in medicine and agriculture, as well as in biomaterials, resins, coatings, and biofuels.[16,17] Although natural rubber (*cis*-1,4-polyisoprene) has been known for a long time, an area that has yet to be explored is its use as monomers to create polymers and copolymers.[18] The extensive structural diversity within this family might explain why they have been underutilized as monomers. Nevertheless, in recent years, there has been a significant increase in the number of articles and patents related to terpene polymerization.[19] Even though polymers derived from terpenes are predominantly elastomers, biological properties, and applications can be expanded when terpenes are used as copolymers.[20]

Limonene and pinene have been the most extensively studied among cyclic terpenes.[21,22] Anionic polymerization is not a good alternative for these building blocks since there is no conjugation.[23] Reactions leading to a cationic or radical mechanism are more appropriate, as these cyclic monomers possess tertiary carbon atoms capable of forming stable carbocations and radicals.[24] The literature[25,26] has already reported copolymerization reactions of limonene via free radicals with acrylate and methacrylate derivatives.

In this work, we aim to combine the benefits of terpenes regarding their organoleptic and biological properties by using them as additives in SLA/MSLA resins containing imidazolium-methacrylate salts as the principal polymeric chain (Figure 1). These new resins are easy to prepare and handle and have immense potential for drug delivery systems and biomedical devices.

Experimental

Materials

Imidazole, 1-methyl-imidazole, 2-methylimidazole, methacrylic acid, methacrylic anhydride, diphenyl (2,4,6-trimethyl benzoyl) phosphine oxide (TPO), α-pinene, *trans*-ethyl cinnamate, safrole, (*R*)-limonene, pyridine, 4-dimethylaminopyridine (DMAP), silica gel 60 for column chromatography and thin layer chromatography (TLC) silica gel plates were obtained from Sigma-Aldrich (Darmstadt, Germany). Glycerol, hydrochloric acid, anhydrous sodium sulfate, and isopropanol were purchased from Labsynth (Diadema, Brazil). All these reagents were of analytical grade and were used without any further purification.

Synthesis of crosslinker

Synthesis of glycerol trimethacrylate (GlycM)

The synthesis of glycerol trimethacrylate (GlycM) followed the methodology described by Fei *et al*.[27] wherein 7.3 mL of glycerol (9.2 g; 0.1 mol), 40 mL of pyridine, 60 mL of methacrylic anhydride, and 125 mg (0.001 mol) of 4-dimethylaminopyridine (DMAP) were sequentially added to a round-bottom flask (Scheme 1). The mixture was stirred at room temperature for 48 h. After this period, the mixture was washed with distilled water and acidified with hydrochloric acid to neutralize the pyridine. Ethyl acetate (2 × 50 mL) was added for extraction. The organic phases were separated, washed with a saturated solution of sodium bicarbonate, dried over anhydrous sodium sulfate, and the solvent was removed using a rotary evaporator. The product was vacuum-dried for 2 h, yielding 24.6 g of glycerol trimethacrylate as a colorless oil (83% yield).

Propane-1,2,3-triyl *tris*(2-methylacrylate) (GlycM)

IR (ATR) ν / cm^{-1} 2971, 1716, 1455, 1135; ^{1}H NMR (600 MHz, $CDCl_3$) δ 2.42 (s, 9H, CH_3), 4.39 (dd, *J* 11.9, 5.9 Hz, 2H, O-CH_2), 4.49 (dd, *J* 11.9, 5.9 Hz, 2H, O-CH_2),

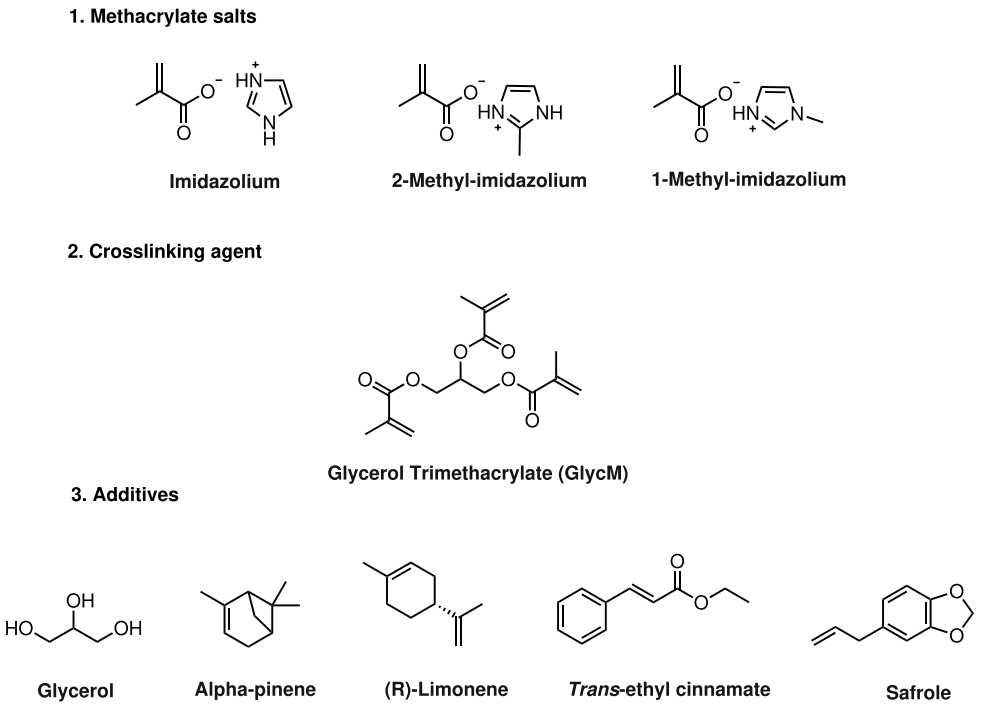

Figure 1. Methacrylate salts, crosslinker and additives used in this work.

5.50-5.53 (m, 1H, CH), 5.65-5.66 (m, 2H, CH_2), 5.65-5.66 (m, 1H, CH_2), 6.19-6.20 (m, 2H, CH_2), 6.19-6.20 (m, 1H, CH_2); ^{13}C NMR (150 MHz, $CDCl_3$) δ 18.2, 18.2, 21.4, 53.4, 62.5, 69.4, 125.35, 126.3, 126.4, 128.3, 135.8, 137.9, 166.3, 166.8 figures presented in the Supplementary Information (SI) section.

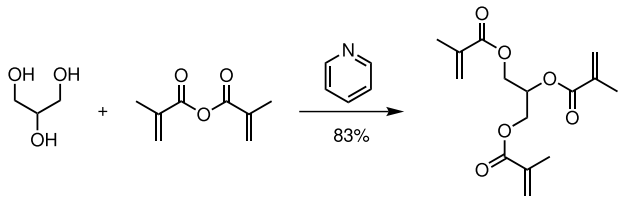

Scheme 1. Glycerol trimethacrylate (GlycM) synthesis.

Resin composition and preparation

Prior to the preparation of the resins, imidazole-based methacrylate salts and their derivatives were synthesized. To achieve this, 0.015 moles (1 eq) of the imidazole derivative were combined with 1.25 mL of methacrylic acid (1.27 g; 0.015 moles, 1 eq) and allowed to react for 10 min in a dark environment with stirring. At the end of this period, 1.1 g of glycerol trimethacrylate (3.75 mmol, 0.25 eq) and 0.07 g of TPO (0.2 mmol, 1 mol%, 0.01 eq) were further introduced in the dark with continued agitation until complete solubilization. The final volume of resin obtained was 1.8 mL without the additives. After following the required procedures, three main formulations of imidazole-based resin were obtained. Adding 0.2 mL of a terpene-based additive resulted in fifteen final resin formulations, each containing a final volume of 2 mL. These formulations are shown in Table 1.

Table 1. Composition of the methacrylate salt resins

Resin	Methacrylate salt	Additive / (10%, v/v)
1.1	imidazolium	glycerol
1.2	imidazolium	α-pinene
1.3	imidazolium	(*R*)-limonene
1.4	imidazolium	*trans*-ethyl cinnamate
1.5	imidazolium	safrole
2.1	2-methyl-imidazolium	glycerol
2.2	2-methyl-imidazolium	α-pinene
2.3	2-methyl-imidazolium	(*R*)-limonene
2.4	2-methyl-imidazolium	*trans*-ethyl cinnamate
2.5	2-methyl-imidazolium	safrole
3.1	1-methyl-imidazolium	glycerol
3.2	1-methyl-imidazolium	α-pinene
3.3	1-methyl-imidazolium	(*R*)-limonene
3.4	1-methyl-imidazolium	*trans*-ethyl cinnamate
3.5	1-methyl-imidazolium	safrole

3D printing

Models of six cylindrical samples measuring 7.5 × 2.5 mm were created in Autodesk Meshmixer[28] and

sliced in Anycubic Photon workshop.[29] These objects were printed to evaluate the printability of the resins. They were all produced in a single printing cycle. Microneedles were also designed using the Autodesk Meshmixer[28] software and sliced in the Anycubic Photon workshop software[29] before printing. The printing parameters involved five initial base layers exposed for 60 s, succeeded by standard layers exposed for 10 s, with a layer height set at 0.05 mm. The printing process was performed using the Anycubic Photon Mono 4K printer[30] (Anycubic, China), enhanced by a modified prototype vat characterized by its minimal resin volume requirement (2 mL minimum). We created the modified vat and platform models inspired by the work of Slowing and co-workers[31] in which they developed a high throughput block adaptor to screen arrays of resin compositions, consuming lower volumes for SLA printing. Our files are available at Cults 3D.[30] Using the adapted vat and platform also required adding an endstop extension to prevent the platform from grounding into the LCD screen (Figure S1, SI section).[32] After printing, objects were cleaned in isopropanol for 1 min, followed by a 1-min post-curing process using an Anycubic Wash'nCure apparatus (Anycubic, China). The AmeraLabs Town[33] calibration file was used with identical parameters for both the needles and the cylinders.

Characterization

Object dimensions were measured using a digital pachymeter. Schore D hardness (Romacci, Brazil) was performed using a portable digital durometer. Mechanical tests were conducted with all resins using specimens for tension and stress (30 × 4 × 2 mm specimens, size 1BB), following the ISO 527-1[34] standards for tensile tests. This test is crucial for estimating Young's modulus, which characterizes the mechanical strength of the material. Tests were also compared with a commercial resin, Anycubic Standard. The tests were carried out using the TRD 22 probe and Emic equipment. TGA (thermogravimetric analysis) was carried out using a TGA-50H (Shimadzu, Japan) under a nitrogen atmosphere at a 10 °C min^{-1} heating rate. FTIR (Fourier transform infrared spectroscopy) analysis was conducted in ATR (attenuated total reflectance) mode with a diamond crystal (Bruker Alpha-II, USA), ^{1}H and ^{13}C nuclear magnetic resonance (NMR) spectra were recorded with a Bruker 600 MHz spectrometer (Bruker, USA)

Resin 1.2 cytocompatibility tests

VERO epithelial cell lines were cultured in RPMI-1640 medium (Sigma-Aldrich, USA) with 10% fetal bovine serum (FBS) (Gibco, Invitrogen, UK) and incubated at 37 °C at 5% CO_2. The cells were lifted with 0.25% trypsin (Gibco, Invitrogen, UK) for 4 min at 37 °C.

Cell viability was determined using the *in vitro* toxicology assay kit, MTT-based (Sigma-Aldrich, USA). To perform the assay, 1×10^6 cells were cultivated in a 6-well plate and incubated for 24 h to ensure cell adhesion. After this time, the 7.5 × 2.5 mm cylindric resin specimen was added to the well, the negative control contained only cells and culture medium. After 24 h of incubation, MTT (3-[4,5-dimethylthiazol-2-yl]-2,5-diphenyltetrazolium bromide, 100 µL from MTT solution at 3 mg mL^{-1} in phosfate buffer solution, PBS) was added to each well, and the plates were incubated at 37 °C in a humid atmosphere containing 95% air and 5% CO_2 for 3 h. Finally, 1 mL of MTT solubilization solution was used to solubilize formazan crystals. Absorbance was measured using a Multiskan SkyHigh plate reader (Thermo Fisher Scientific, USA) at 570 nm. The experiments were performed in triplicate.

Results and Discussion

The main objective of this work is to develop new and easy-to-handle resins for stereolithography and use in biomedical 3D printing. Imidazole-derived methacrylate salts were chosen as the main chain, and glycerol trimethacrylate was selected as the crosslinker. Using a crosslinking agent in these cases addresses the issue that imidazolium salt resins are water-soluble. By using the crosslinker, this problem can be circumvented.

Glycerol trimethacrylate is a crosslinking agent with three growth sites capable of increasing the density of the polymer network, aiming for more rigid materials. Due to its biocompatibility[35] and ease of synthesis, glycerol trimethacrylate was the crosslinker of choice. Terpenes were then added to study the effects of their addition on the mechanical properties of these new resins. Combining these factors, 15 resins could be prepared and tested (Table 1). A schematic view of this network can be seen in Figure 2.

Figure 3 displays the Shore D hardness measurement values for all prepared resins. All resins demonstrated good printability (Figure S2, SI section) once the objects printed had dimensions like those of commercial resin. Regarding the terpene additives α-(–)-pinene, (*R*)-limonene, *trans*-ethyl cinnamate, and safrole, it was noticed that the additives α-pinene and (*R*)-limonene increased the hardness of the resins compared to the resin without additives, while safrole had the opposite effect. Almost all the mentioned resins exhibited a higher Shore D hardness than commercial resin, except for resins 1.5 and 2.5 (due to the presence of safrole as

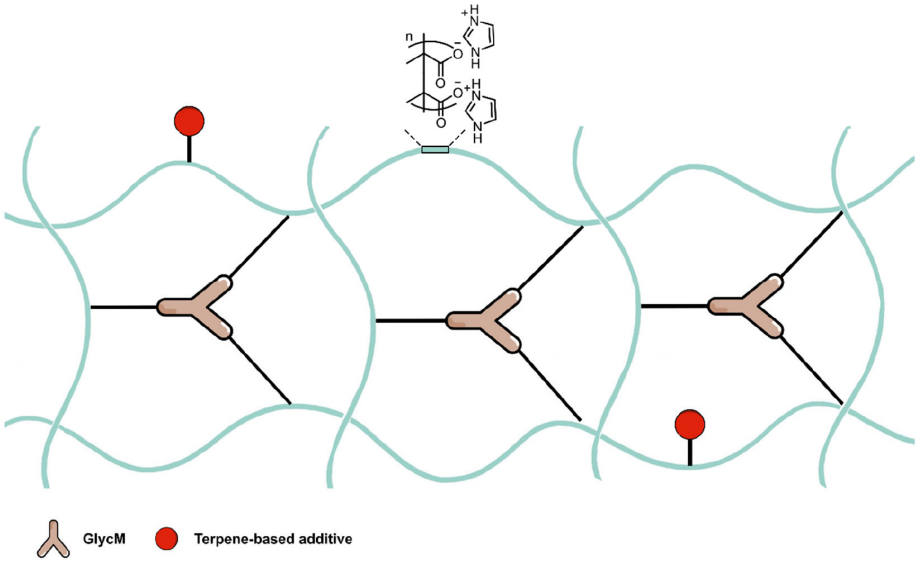

Figure 2. Simplified schematic view of our resin network.

an additive). Regarding the width and height measurements of the discs, the width for all resins showed values very close to the commercial resin, and they were also quite similar to the virtual model (Table S1, SI section). The behavior in terms of height was identical, except that none closely matched the virtual model in this measurement.

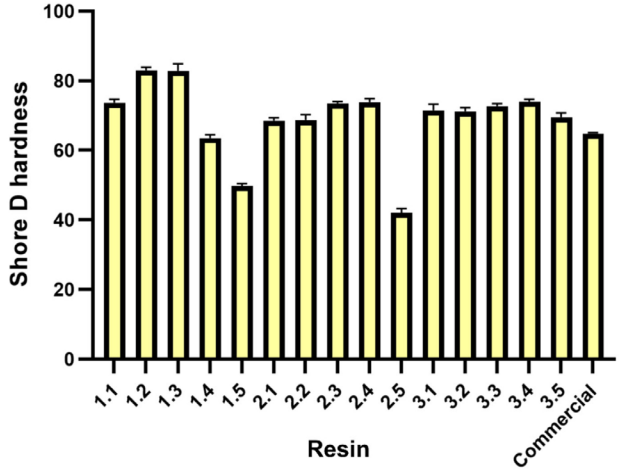

Figure 3. Shore D hardness values of the resins containing the additives.

A standard specimen was employed for each resin to conduct the tensile stress tests. The specimens were 3D printed along the x-axis to ensure the layers were perpendicular to the fracture stress, resulting in increased failure resistance. This approach has been previously outlined in published works[36] and is considered a crucial aspect of the testing process.

When comparing resins containing the blank control (glycerol), resins 1.1, 2.1, and 3.1, the influence of derived imidazole salts on mechanical tests can be determined. The resin containing the imidazole salt (1.1) had a better Young's modulus than resins 2.1 and 3.1, and the resin formulations containing 1-methyl-imidazolium had the lowest ratings overall. This may be due to the loss of the hydrogen bond donor group in 1-methylimidazole compared to unsubstituted imidazole, resulting in weaker intermolecular interactions.[37] Additionally, steric effects related to the introduction of the methyl group can increase hydrophobic interactions, which would also result in weaker mechanical properties.[38]

Combining methacrylate salt resins with the additives α-(–)-pinene and (*R*)-limonene also proved to be beneficial in increasing fracture resistance, as resins 1.2 and 2.3 presented an elasticity modulus comparable to the commercial resin (Figure 4).

The mechanical data clearly show that imidazole salts and 2-methylimidazole provide suitable resins. In contrast, 1-methylimidazole salts do not yield results as good as those of their sibling compounds. The reasons still seem obscure since 1-methylimidazole salts are also used to prepare ionic liquids and are slightly more basic than the other derivatives. These results provide an economic advantage for imidazole and 2-methylimidazole salts, as they exhibited good mechanical properties and good printability, and their bases cost less than half the price of 1-methylimidazole, leading to cheaper final products.

The infrared spectra of the printed resin and its precursors provide valuable information regarding the formation of the resin and the GlycM monomer synthesis. The synthesis of the GlycM monomer through glycerol methacrylation (purple line) is supported by a band around 1720 cm^{-1}. This band is characteristic of carbonyl (C=O) stretching vibrations in α and β-unsaturated esters,[39] confirming

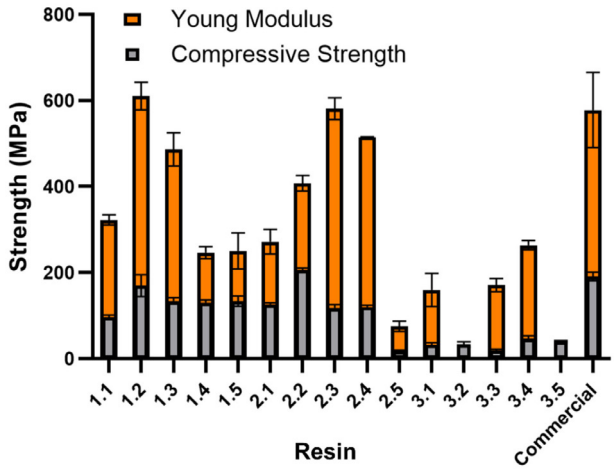

Figure 4. Mechanical tests for printed specimens (measurements in MPa).

the incorporation of methacrylate groups. Furthermore, the absence of the wide band corresponding to hydroxyl groups[39] between 3650- 3000 cm^{-1} in the GlycM spectrum confirms that all hydroxyl groups have been modified and the functionalization was fully completed (Figure 5).

The alkene bands found in the precursors, methacrylic acid (blue line) and GlycM (green line), are discussed below. The absence of the band around 1628 cm^{-1}, is attributed to C=C stretching vibrations.[39] The printed resin 1.1 (black line) spectrum confirms that alkene double bonds are consumed during the photopolymerization process during resin printing.

Regarding imidazole, the band related to the N–H vibrational stretching around 3125 cm^{-1} and C=C vibrational stretching of the imidazole ring in 1560 cm^{-1} is observed. As expected, both bands remain in the 1.1 printed resin spectrum.[39]

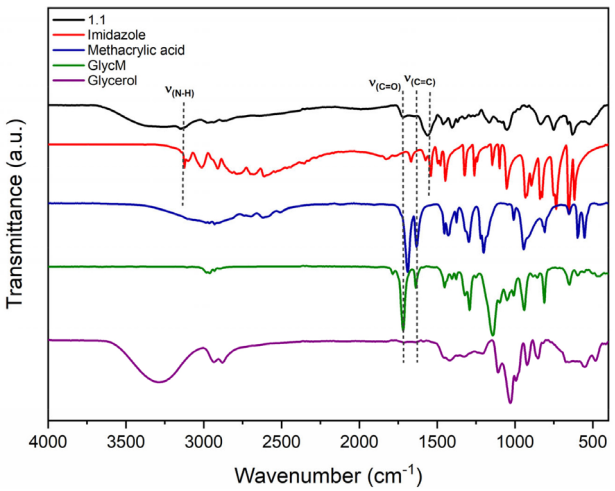

Figure 5. FTIR spectra of cured resin 1.1 (black line) compared to its precursors: imidazole (red line), methacrylic acid (blue line), glycerol (purple line), and monomer GlycM (green line).

Three main resin compositions were synthesized by varying the methacrylate salt source, as shown in Table 1. Group 1 uses an imidazole salt, while groups 2 and 3 use 2-methyl-imidazolium and 1-methyl-imidazolium, respectively. Figure 6 shows FTIR spectra for resins 1.1, 2.1 and 3.1. In all of them, the vibrational stretching of the carbonyl derived from the methacrylate salt and GlycM is observed at 1720 cm^{-1}, as mentioned before. The C=N and C=C stretching vibrations of the imidazole ring are also noticeable at approximately 1638 and 1560 cm^{-1}, respectively. These observations and findings can be extrapolated to the other resin spectra, and additional data can be found in the SI section.

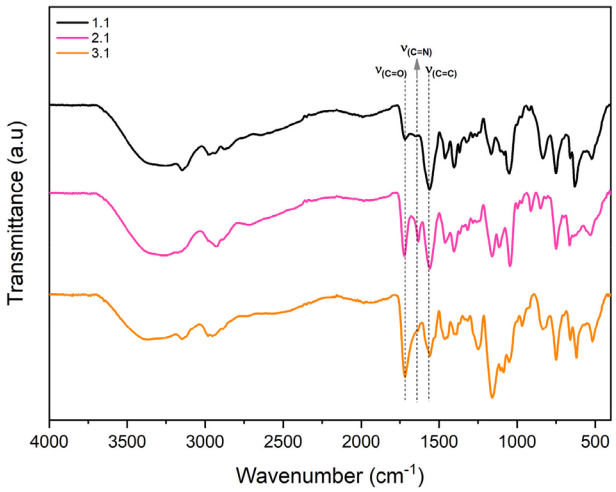

Figure 6. FTIR spectra of cured resin 1.1 (black line), 2.1 (pink line), and 3.1 (orange line).

Thermal gravimetric analysis was performed to identify the thermal stability of printed resins. Thermograms and DTG (derivative thermogravimetry) curves are presented in Figure 7. The thermal stability of the material is attained at 450 °C. Three steps of decomposition were observed for the printed resins. The first decomposition step was observed from 57 to 129 °C and may be associated with the loss of moisture and volatile terpenes associated with the resins.[40] The second decomposition step occurs between 220 and 240 °C and is associated with the degradation of imidazole groups.[41] During the third stage, the maximum temperature (T_{max}) ranged from 416 to 435 °C, and a mass loss of around 75% was attributed to the methacrylate groups.[42]

All resins exhibit similar thermogravimetric profiles, with the resins containing 1-methyl-imidazole salt being the most thermally stable. The methyl-imidazole salt resins, whether in position 1 or 2 of the heterocycle, conferred better heat resistance, as there is an increase in T_{max} in groups 2 and 3 resins compared to group 1 resins. However,

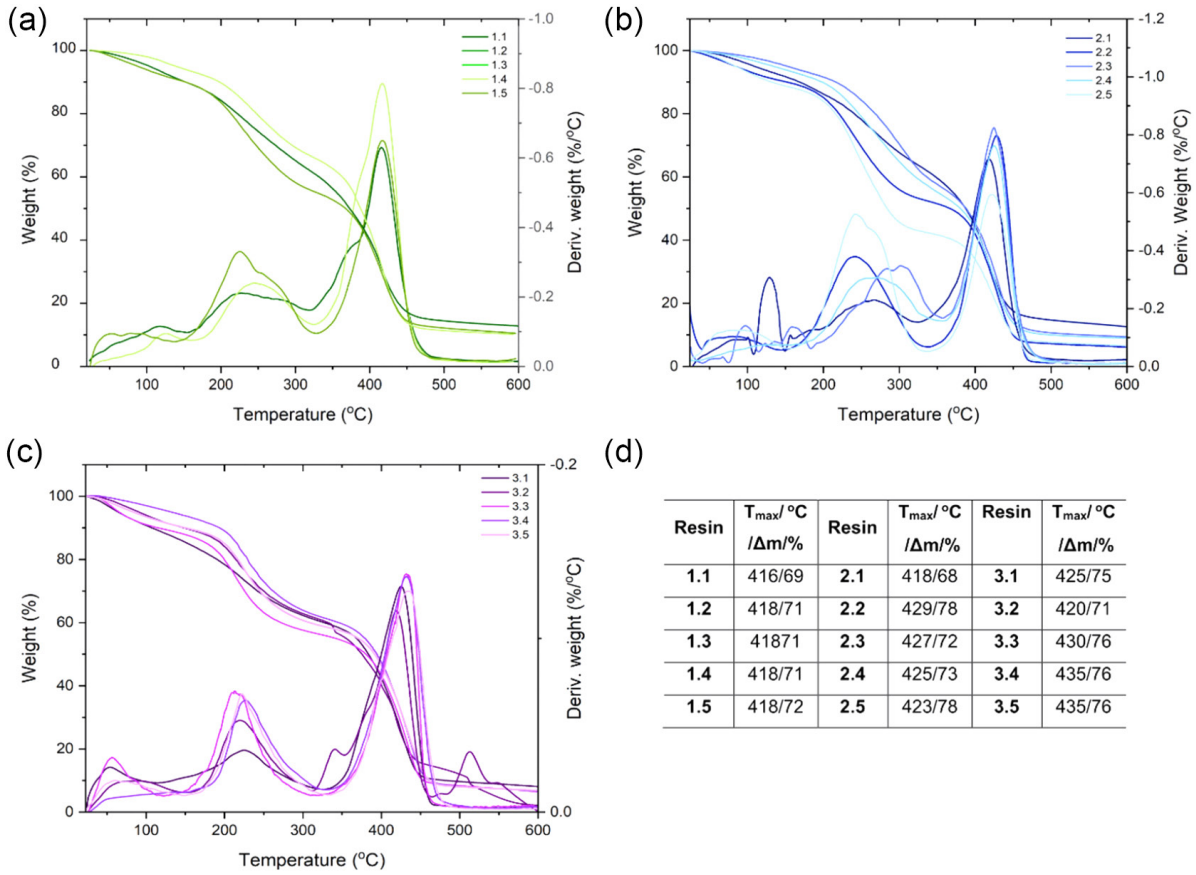

Resin	T_{max}/ °C /Δm/%	Resin	T_{max}/ °C /Δm/%	Resin	T_{max}/ °C /Δm/%
1.1	416/69	**2.1**	418/68	**3.1**	425/75
1.2	418/71	**2.2**	429/78	**3.2**	420/71
1.3	41871	**2.3**	427/72	**3.3**	430/76
1.4	418/71	**2.4**	425/73	**3.4**	435/76
1.5	418/72	**2.5**	423/78	**3.5**	435/76

Figure 7. TG and DTG curves of printed resins for groups 1 (a), 2 (b), and 3 (c) and their respective maximum temperature (T_{max}) and mass loss (Δm) (d).

since the difference is approximately 10 to 15 degrees and all resins showed good resistance, losing most of the organic material above 400 degrees, it can be considered that group 1 resins, especially those containing α-pinene or (*R*)-limonene in their compositions, are superior to the others. These results prove that the material exhibits thermal stability up to 400 °C, which is advantageous for conventional sterilization processes requiring high temperatures, such as autoclaving (ca. 121 °C).

Although they did not exhibit the best performance in thermogravimetric characterization, the resins from group 1 containing limonene or α-pinene showed the best mechanical characteristics of a suitable resin, surpassing the standard commercial resin in tests. Indeed, both α-pinene and limonene can strengthen the resin structure by forming cross-links with the monomers used. Although cationic polymerization is the preferred mechanism for these alkenes, they can also form radicals and undergo radical polymerization[43] with the monomers utilized here. This copolymerization proves to be beneficial for these materials.

Our idea with this work was to develop simple, easy-to-prepare, and biocompatible resins for biomedical devices. To do this, we used the imidazole salt chain as the main chain, glycerol trimethacrylate as the crosslinker, and terpenes to enhance the mechanical characteristics of these new resins. As it became clear that materials reinforced with α-pinene and limonene were the best candidates for resins, we believe that these terpenes reacted with the methacrylate, being incorporated into the material and improving its physical characteristics. In fact, resins containing limonene and thiols can undergo thiol-ene reactions aimed at polymerization between the radical formed at the sulfur atom and the terminal double bond in limonene.[44,45] On the other hand, α-pinene was used as a self-crosslinking agent when methacrylate was used, producing a fully renewable poly high internal phase emulsion (polyHIPE) without the need for additional crosslinking agents. This showcases the potential of αPMA as a versatile and sustainable monomer.[46]

Therefore, to evaluate the resolution of one of these resins, specifically resin 1.2, it was decided to print the calibration piece from AmeraLabs. The AmeraLabs[33] printing test offers valuable insights for calibrating printer settings and resin resolution issues. In Figure 8, the AmeraLabs test was conducted using the resin that yielded the best results in mechanical tests (1.2). The complete AmeraLabs Town[33] object is shown in Figures 8a and 8b from the front and back views, respectively. Tests

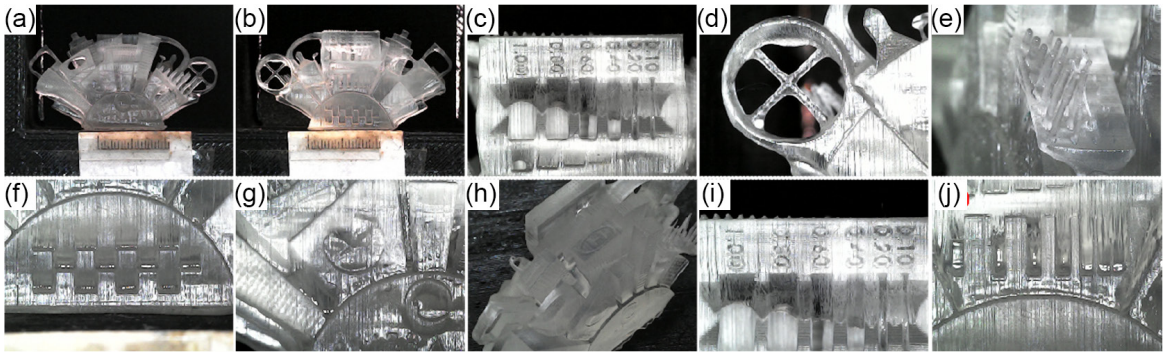

Figure 8. AmeraLabs town 3D printer resin test.

assessing excessive resin exposure during printing or resin resolution (Figure 8c) indicate that resin 1.2 exhibited minimal resolution issues, as evidenced by gaps ranging from 1.0 to 0.1 mm. The cross-shaped bridges (Figure 8d) and pillars (Figure 8e) evaluate material hardness and toughness, which are crucial for 3D printing models with intricate details. The absence of some pillars (the last row) indicates that our resin formulation may not present the hardness and toughness needed or that there needs to be more resolution in both the resin and printer. As observed in our printed model, tests in Figures 8f and 8g verify whether the resin reproduces sharp edges and proper depth accurately. Resin viscosity is assessed by its ability to drain out of spaces among buildings, as seen in Figure 8h. The resolution of the printing system is evaluated by its ability to form small cylinders ranging from 0.20 to 0.05 mm. Still, it is challenging to observe all cylinders, even in commercial resin, due to the inherent resolution limitations of the printer (Figure 8i). The final test evaluates the slicing process of the 3D design; an object with uniform height where all ledges are visible indicates that there were no slicing errors, as seen in Figure 8j.

Knowing that the formulated resins, especially resin 1.2, with the best overall results, passed the printing and resolution tests as seen previously, it was decided to apply it in a medical device. The resin was used to produce star-shaped microneedles. We chose the star-shaped microneedle according to a study by De Martino *et al.*[47] The star-shaped microneedle demonstrated better penetration and release capabilities than other shapes, such as circles, triangles, and squares.[47] The star-shaped microneedles were designed and tested using resin 1.2, as shown in Figure 9. The microneedle base was 10 × 10 × 0.5 mm and comprised 81 microneedles, each 1 mm high. The sample shows a translucent appearance even after the post-curing process, and it is possible to observe that the star-shaped structure was obtained after printing, and the tip remains sharp as in the 3D design. The microneedles presented an average size of 0.5 mm, shorter than the length of the virtual model, which was set at 1 mm. This happens because the light that solidifies the material scatters across neighboring pixels on the LCD panel. The light accumulates in larger areas, resulting in more light *per* unit area than in smaller areas. Solidifying objects with small dimensions makes it challenging because more than the light intensity may be needed to achieve the minimum dose required for polymerization.[48] In fabricating printed microneedles intended for transdermal drug delivery, it is advisable to aim for needle heights falling within the 800-600 μm range. This target range is conducive to minimizing discomfort during application. It is noteworthy that needles surpassing the 1000 μm threshold are linked with heightened pain sensations. This phenomenon can be attributed to capillary networks situated at a depth of approximately 1 mm within the papillary dermal region.[49] This way, the devices developed herein show potential for transdermal drug delivery.

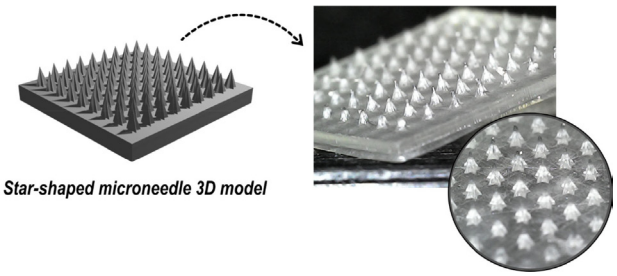

Figure 9. Star-shaped microneedle 3D model and printed version using resin 1.2.

Finally, to evaluate resin 1.2 cytocompatibility, cylindrical objects were tested in the VERO cell line (ATCC CCL-81) using the MTT method.[50] The result is shown in Figure 10, in which the percentage of cell viability for VERO cells after treatment with the resin was 82.3% compared to the control (100% cell viability). This indicates that the resin exhibits good biocompatibility with normal cells, paving the way for developing drug-delivery devices.

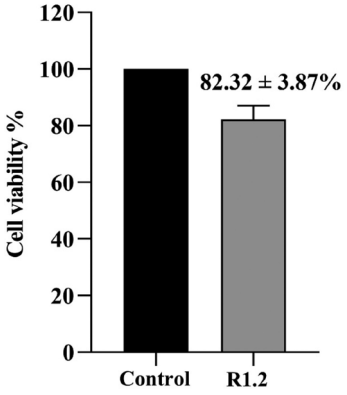

Figure 10. Viability of the VERO cells after 24 h of exposure to resin 1.2 specimens.

Conclusions

We described the development of novel 3D printable resins composed mainly of methacrylate salts as monomers and trimethacrylated glycerol (GlycM) as a crosslinking agent. Terpene-based additives were incorporated to improve resin quality. These resins are easy to prepare, have a low cost of production, and no solvent is used in their preparation. Thermal gravimetric analysis indicates thermal resin stability up to 450 °C. Adding terpenes as copolymers introduced better fracture resistance and enhanced organoleptic properties. The additives α-pinene and (*R*)-limonene positively favored the resin formulation to have a higher modulus of elasticity than the commercial resin. On the other hand, adding safrole oppositely contributed to this effect, leading to fragile final products after the printing process. When comparing the methacrylate salts, 1-methyl imidazolium presented the lowest values of Young's modulus, indicating lower fracture resistance than all resins from group 3. This research opens possibilities for developing advanced 3D printing materials with improved functionality, offering potential applications in medicine and biotechnology, such as the design of microneedles for drug delivery.

Supplementary Information

Supplementary information, including IR spectra, mechanical test data, NMR spectra, and details on the mini platform and vat models, is available free of charge at http://jbcs.sbq.org.br as a PDF file.

Acknowledgments

We thank Fundação de Amparo a Ciência e Tecnologia do Estado de Pernambuco (FACEPE) for funding this work through APQ-1003.06/22 and PROPG/Universidade Federal do Pernambuco (UFPE, grant 09/2023). I. M. S. L. acknowledges Coordenação de Aperfeiçoamento de Pessoal de Nível Superior (CAPES) for the graduate fellowship, A. G. V. acknowledges CAPES-RIMA for the graduate fellowship, and L. G. M. acknowledges CAPES-RIMA for the postdoctoral fellowship.

Author Contributions

Ilária M. S. Lins was responbible for data curation, formal analysis, investigation, software, validation, writing original draft; Anderson G. Vieira for data curation, formal analysis, investigation; Rubson P. S. Ribeiro for data curation, formal analysis, investigation; Dayane K. N. Santos for data curation, investigation; Larissa G. Maciel for conceptualization, data curation, formal analysis, investigation, software, validation, visualization; Petrus A. Santa-Cruz for formal analysis, project administration, resources, writing (review and editing); Severino Alves Júnior for formal analysis, funding acquisition, project administration, resources, writing (review and editing); Janaína V. dos Anjos for conceptualization, formal analysis, funding acquisition, project administration, resources, writing (review and editing).

References

1. Li, B.; Zhang, M.; Lu, Q.; Zhang, B.; Miao, Z.; Li, L.; Zheng, T.; Liu, P.; *BioMed Res. Int.* **2022**, *2022*, 8759060. [Crossref]
2. Timofticiuc, I. A.; Călinescu, O.; Iftime, A.; Dragosloveanu, S.; Caruntu, A.; Scheau, A. E.; Badarau, I. A.; Didilescu, A. C.; Caruntu, C.; Scheau, C.; *J. Funct. Biomater.* **2024**, *15*, 7. [Crossref]
3. Wang, X.; Liu, J.; Zhang, Y.; Kristiansen, P. M.; Islam, A.; Gilchrist, M.; Zhang, N.; *Virtual Phys. Prototyping* **2023**, *18*, 1. [Crossref]
4. Deshmane, S.; Kendre, P.; Mahajan, H.; Jain, S.; *Drug Dev. Ind. Pharm.* **2021**, *47*, 1362. [Crossref]
5. Chowdhury, S.; Yadaiah, N.; Prakash, C.; Ramakrishna, S.; Dixit, S.; Gupta, L. R.; Buddhi, D.; *J. Mater. Res. Technol.* **2022**, *20*, 2109. [Crossref]
6. Kowsari, K.; Akbari, S.; Wang, D.; Fang, N. X.; Ge, Q.; *3D Print. Addit. Manuf.* **2018**, *5*, 185. [Crossref]
7. Park, S.; Shou, W.; Makatura, L.; Matusik, W.; Fu, K. K.; *Matter* **2022**, *5*, 43. [Crossref]
8. Ahmed, I.; Sullivan, K.; Priye, A.; *Biosensors* **2022**, *12*, 652. [Crossref]
9. Ribas-Massonis, A.; Cicujano, M.; Duran, J.; Besalú, E.; Poater, A.; *Polymers* **2022**, *14*, 2856. [Crossref]
10. Fertier, L.; Koleilat, H.; Stemmelen, M.; Giani, O.; Joly-Duhamel, C.; Lapinte, V.; Robin, J. J.; *Prog. Polym. Sci.* **2013**, *38*, 932. [Crossref]
11. Pirman, T.; Ocepek, M.; Likozar, B.; *Ind. Eng. Chem. Res.* **2021**, *60*, 9347. [Crossref]

12. Jorge, J. H.; Giampaolo, E. T.; Machado, A. L.; Vergani, C. E.; *J. Prosthet. Dent.* **2003**, *90*, 190. [Crossref]
13. Kabanov, V. A.; Topchiev, D. A.; Karaputadze, T. M.; *J. Polym. Sci., Part C: Polym. Symp.* **1973**, *42*, 173. [Crossref]
14. de Albuquerque, A. S.; Vaz, E. C. R.; dos Anjos, J. V.; Santa-Cruz, P. A.; *Opt. Mater.: X* **2024**, *21*, 100283. [Crossref]
15. Andrei, G. Ș.; Andrei, B. F.; Roxana, P. R.; *Mini-Rev. Med. Chem.* **2021**, *21*, 1380. [Crossref]
16. Masyita, A.; Sari, R. M.; Astuti, A. D.; Yasir, B.; Rumata, N. R.; Emran, T. B.; Nainu, F.; Simal-Gandara, J.; *Food Chem.* **2022**, *13*, 100217. [Crossref]
17. Mosquera, M. E. G.; Jiménez, G.; Tabernero, V.; Vinueza-Vaca, J.; García-Estrada, C.; Kosalková, K.; Sola-Landa, A.; Monje, B.; Acosta, C.; Alonso, R.; Valera, M. A.; *Sustainable Chem.* **2021**, *2*, 467. [Crossref]
18. Palenzuela, M.; Sánchez-Roa, D.; Damián, J.; Sessini, V.; Mosquera, M. E. G.; *Adv. Organomet. Chem.* **2021**, *75*, 55. [Crossref]
19. Winnacker, M.; Rieger, B.; *ChemSusChem* **2015**, *8*, 2455. [Crossref]
20. Sahu, P.; Bhowmick, A. K.; Kali, G.; *Processes* **2020**, *8*, 553. [Crossref]
21. Vieira, A. J.; Beserra, F. P.; Souza, M. C.; Totti, B. M.; Rozza, A. L.; *Chem.-Biol. Interact.* **2018**, *283*, 97. [Crossref]
22. Winnacker, M.; *Angew. Chem., Int. Ed.* **2018**, *57*, 14362. [Crossref]
23. Ishizone, T.; Goseki, R. In *Encyclopedia of Polymeric Nanomaterials*; Kobayashi, S.; Müllen, K., eds.; Springer: Berlin, Heidelberg, 2014, p. 1. [Crossref]
24. Taburet, N.; Zawadzki, L.; Vayre, M.; Blumstein, D.; Gac, S. Le; Boy, F.; Raynal, M.; Labroue, S.; Crétaux, J. F.; Femenias, P.; *Polymers* **2020**, *12*, 2146. [Crossref]
25. Sharma, S.; Srivastava, A. K.; *J. Macromol. Sci., Part A: Pure Appl. Chem.* **2003**, *40A*, 593. [Crossref]
26. Doiuchi, T.; Yamaguchi, H.; Minoura, Y.; *Eur. Polym. J.* **1981**, *17*, 961. [Crossref]
27. Fei, M.; Liu, T.; Fu, T.; Zhang, J.; Wu, Y.; Qiu, R.; Liu, W.; *ACS Sustainable Chem. Eng.* **2019**, *7*, 17808. [Crossref]
28. *Autodesk Meshmixer*, version 3.5.474; Autodesk Inc., Portland, OR, USA, 2017.
29. *Anycubic Photon Workshop 3D Slicer Software*, version 3.1.4; Anycubic Co. Ltd., Shenzen, China, 2023.
30. Cults 3D, *Mini Vat and Platform for Anycubic Photon Mono 4k*, https://cults3d.com/en/3d-model/tool/mini-vat-and-platform-for-anycubic-photon-mono-4k, accessed in October 2024.
31. Manzano, J. S.; Wang, H.; Slowing, I. I.; *ACS Appl. Polym. Mater.* **2019**, *1*, 2890. [Crossref]
32. Cults 3D, *Endstop for Anycubic Photon Mono 4k*, https://cults3d.com/en/3d-model/tool/endstop-for-anycubic-photon-mono-4k, accessed in October 2024.
33. AmeraLabs, *Ameralabs Town Guide & STL*, https://ameralabs.com/blog/town-calibration-part/, accessed in October 2024.
34. ISO 527-1:2019: *Plastics - Determination of Tensile Properties*, ISO: Geneva, 2019.
35. Hong, S. H.; Kim, J. E.; Kim, Y. K.; Minai-Tehrani, A.; Shin, J. Y.; Kang, B.; Kim, H. J.; Cho, C. S.; Chae, C.; Jiang, H. L.; Cho, M. H.; *Int. J. Nanomed.* **2012**, *7*, 2293. [Crossref]
36. Schittecatte, L.; Geertsen, V.; Bonamy, D.; Nguyen, T.; Guenoun, P.; *MRS Commun.* **2023**, *13*, 357. [Crossref]
37. Shin, J. Y.; Wang, Y. L.; Yamada, S. A.; Hung, S. T.; Fayer, M. D.; *J. Phys. Chem. B* **2019**, *123*, 2094. [Crossref]
38. Gu, S.; Gao, Y.; Ren, X.; Yu, J.; Duan, L.; Gao, G.; *J. Polym. Sci., Part B: Polym. Phys.* **2018**, *56*, 1505. [Crossref]
39. Silverstein, R. M.; Webster, F. X.; Kiembe, D. J.; *Spectrometric Identification of Organic Compunds*, 5th ed.; John Wiley & Sons Inc: USA, 2005.
40. Zeinali, R.; Del Valle, L. J.; Franco, L.; Yousef, I.; Rintjema, J.; Alemán, C.; Bravo, F.; Kleij, A. W.; Puiggalí, J.; *Polymers* **2022**, *14*, 161. [Crossref]
41. Elangovan, K.; Senthil, A.; Vinitha, G.; *J. Mater. Sci.: Mater. Electron.* **2019**, *30*, 13664. [Crossref]
42. Gałka, P.; Kowalonek, J.; Kaczmarek, H.; *J. Therm. Anal. Calorim.* **2014**, *115*, 1387. [Crossref]
43. Rodrigues, P. R.; Gonçalves, S. A.; Vieira, R. P.; *Eur. Polym. J.* **2021**, *147*, 110303. [Crossref]
44. Claudino, M.; Mathevet, J. M.; Jonsson, M.; Johansson, M.; *Polym. Chem.* **2014**, *5*, 3245. [Crossref]
45. Chiaradia, V.; Pensa, E.; Machado, T. O.; Dove, A. P.; *ACS Sustainable Chem. Eng.* **2024**, *12*, 6904. [Crossref]
46. Monaghan, O. R.; Skowron, S. T.; Moore, J. C.; Pin-Nó, M.; Kortsen, K.; Atkinson, R. L.; Krumins, E.; Lentz, J. C.; Machado, F.; Onat, Z.; Brookfield, A.; Collison, D.; Khlobystov, A. N.; De Focatiis, D.; Irvine, D. J.; Taresco, V.; Stockman, R. A.; Howdle, S. M.; *Polym. Chem.* **2022**, *13*, 5557. [Crossref]
47. de Martino, S.; Battisti, M.; Napolitano, F.; Palladino, A.; Serpico, L.; Amendola, E.; Martone, A.; de Girolamo, P.; Squillace, A.; Dardano, P.; de Stefano, L.; Dello Iacono, S.; *Biomater. Adv.* **2022**, *142*, 213169. [Crossref]
48. Brasselet, S.; Ferrand, P.; Kress, A.; *Springer Ser. Fluoresc.* **2013**, *13*, 311. [Crossref]
49. Zhu, J.; Zhou, X.; Kim, H. J.; Qu, M.; Jiang, X.; Lee, K. J.; Ren, L.; Wu, Q.; Wang, C.; Zhu, X.; Tebon, P.; Zhang, S.; Lee, J.; Ashammakhi, N.; Ahadian, S.; Dokmeci, M. R.; Gu, Z.; Sun, W.; Khademhosseini, A.; *Small* **2020**, *16*, e1905910. [Crossref]
50. Guerrero-Gironés, J.; López-García, S.; Pecci-Lloret, M. R.; Pecci-Lloret, M. P.; Rodríguez Lozano, F. J.; García-Bernal, D.; *J. Dent.* **2022**, *123*, 104163. [Crossref]

Submitted: July 23, 2024
Published online: October 23, 2024